Properties of polarization echoes in piezoelectric powders

1997 J. Phys.: Condens. Matter 9 9361

(http://iopscience.iop.org/0953-8984/9/43/020)

J. Phys.: Condens. Matter **9** (1997) 9361–9379. Printed in the UK PII: S0953-8984(97)79437-2

Properties of polarization echoes in piezoelectric powders

T Ya Asadullin† and Ya Ya Asadullin‡

† Kazan State Technical University, Department of General Physics, Karl Marx Street 10, Kazan 420111, Russia

‡ Kazan Physical-Technical Institute, Kazan Scientific Centre of RAS, Sibirskii Trakt 10/7, Kazan 420029, Russia

Received 11 November 1996, in final form 20 June 1997

Abstract. A theoretical description is given for nonlinear formation mechanisms and properties of the polarization echoes in piezoelectric powders, earlier experimentally investigated in both the radiofrequency (rf) and the microwave (mw) frequency domains. For rf echoes, a phenomenological model is elaborated for dynamics of dislocations in mechanically vibrating piezoelectric particles resonantly excited by short-duration pulses of rf electric field. The model includes both the reversible and irreversible moving groups of dislocations generated by Frank–Read sources. The amplitude-dependent frequency change and amplitude-dependent damping obtained by use of this model constitute two of the three nonlinear mechanisms responsible for the formation of the polarization echoes in piezoelectric powders with the signals naturally consisting of both the dynamic and the memory components. As a third type of nonlinearity, the field–mode interaction, we take the nonlinear electrostriction. For mw echoes, it is proposed that the lack of memory components in the echoes is a consequence of absence of mobile dislocations in the powder material used. We suggest a somewhat modified form of the nonlinear mechanisms related to the pure lattice anharmonicity: amplitude-dependent dispersion and damping. General expressions for two-pulse rf echoes and mw echoes are derived by using *together* all three types of nonlinear mechanism inherent in each frequency domain. The numerical analysis of these expressions as a function of the pulse amplitudes, the pulse widths and the pulse separation shows good agreement between the theory and the existing experiments in a broad range of amplitudes and widths of the pulses. As a result, several important material constants relevant to the nonlinear mechanisms in SiO_2 (rf domain) and in ZnO (mw domain) are estimated.

1. Introduction

Since the discovery [1] of the polarization echoes in piezoelectric powders, many experimental investigations of amplitude, time and phase properties of this phenomenon have been carried out by several groups of investigators. The most important characteristic of any echo is its dependence on the pulse separation τ. It was found and studied in detail by Fossheim *et al* [2] that instead of the monotonic decay usually expected in echo phenomena, the time dependence of the radiofrequency (rf) echo in quartz powders has pronounced extrema. Similar behaviour of the two-pulse echo was observed also in ZnO powders at microwave (mw) frequencies [2]. Note that such time dependence takes place also in cyclotron echoes in plasmas [3], NMR echoes in antiferromagnetics [4] and photon echoes in crystals [5]. That is, we deal with the peculiarity of echoes general for different physical systems.

On the other hand, it is appropriate to mention here that the memory echoes are observed only in the rf domain. Therefore, we may suppose that the polarization echoes at rf and at microwave frequencies are caused by nonlinear mechanisms of different physical origin.

0953-8984/97/439361+19$19.50

The purpose of this paper is to ascertain the nonlinear mechanisms of both rf and mw polarization echoes in piezoelectric powders, elaborate the quantitative theory and on the basis of the theory to explain the important properties of this phenomenon.

2. RF echoes. Model for nonlinear mechanisms

From the usual wave equation for the strain field $s(x,t)$ in an individual powder particle

$$\ddot{s} + 2\Gamma_0\dot{s} - \frac{G}{\rho}s_{xx} = F(x,t) = F_l(x,t) + F_{nl}(x,t) \tag{1}$$

it follows that the three general types of nonlinear mechanism [6] for the case of the polarization echoes in powders are (i) nonlinear excitation of the mechanical oscillations in the particles by the applied pulses (nonlinear interaction $F_{nl}(x,t)$), (ii) amplitude dependence of the normal mode frequency Ω (or, in other words, of the elastic modulus G) and (iii) amplitude dependence of the damping $\Gamma = T_2^{-1}$. Various physical factors and processes may contribute to these mechanisms with different degrees of efficiency.

The nonlinear interaction mechanism ('parametric field–mode interaction') is that by which the applied field couples to the excited mode of mechanical oscillations. The lowest-order term in the expansion of the internal energy over the strain s and the internal field E_{in} describing this interaction is of the form [2, 7]

$$U = \tfrac{1}{2}\gamma_6 E_{in}^2 s^2 \tag{2}$$

where γ_6 is the constant of the nonlinear electrostriction. Another type of nonlinear interaction is related to the motion of charged dislocations (see below).

The existence of the memory echoes in piezoelectric powders was attributed to the motion of dislocations [8–15]. Here we mean the mobile dislocations created during the preparation of powder samples. In the case of rf echoes [2], the powder particles have size $\sim$0.01 cm and were obtained by grinding of single crystals. As a result, a density of dislocations $\geqslant 10^{10}$ cm^{-2} is created so that a particle contains 10^5–10^6 lines of dislocations.

Note that in metal powders [16, 17], too, strong signals of the polarization echoes are observed in samples prepared by filing from the bulk materials. The echoes are weak or not found in the commercial powders not containing mobile dislocations.

In the presence of mobile dislocations, the resulting strain in the particle, $s(x,t)$, is made up of two contributions, the elastic strain $s_e(x,t)$ and the dislocation strain, $s_d(x,t)$, due to the motion of the dislocations under the influence of the stress $\sigma(x,t)$ excited by the applied pulse. As a result, the dislocation motion causes a change in the modulus, $G = G_0 - \Delta G_d$, and an additional internal friction, $\Gamma = \Gamma_0 + \Gamma_d$, where G_0 and Γ_0 are related to the dislocationless crystal. The qualitative model and phenomenological theory of dislocation losses described below present the natural development of our previous work [11–13] on the subject.

Depending on the character of dislocation motion, there are various types of contribution to ΔG_d and Γ_d. For low stresses, dislocations bow out between weak pinning points, and the dislocation contributions to ΔG_d and to Γ_d are amplitude independent. They are given by well known expressions [18]

$$\Gamma_{d0} = \frac{\Lambda b^2 G\Omega^2 B}{2A^2[(\Omega_d^2 - \Omega^2)^2 + (\Omega B/A)^2]} \qquad \Delta G_{d0} = \frac{\Lambda b^2 G^2(\Omega_d^2 - \Omega^2)}{A[(\Omega_d^2 - \Omega^2)^2 + (\Omega B/A)^2]}$$
$$\Omega_d = \pi^2 C/l^2 A. \tag{3}$$

Here, b is the magnitude of the Burgers vector, $\Lambda = N_0 l$ the total length of mobile dislocations per unit volume, l the distance between weak pinning points, N_0 the number of loops, A the effective mass per unit length of dislocation, B the damping force per unit length and unit velocity and C is the line tension of the dislocation.

As soon as the stress amplitude becomes large enough, break-away from the weak pins occurs. The dislocations are now vibrating between the dislocation network nodes (which are considered to be strong pinning points) with the full network loop length L. For still larger stresses produced during the applied pulses, the dislocations are bowed out sufficiently far to initiate the operation of a Frank–Read source, resulting in extensive dislocation multiplication. An increase of the dislocation density due to the operation of Frank–Read sources leads to the sharp increase of Γ_d and ΔG_d at the rising edge of the applied pulse [19]. The piling up of these dislocations against an obstacle causes the fast decrease of Γ_d and ΔG_d to a some quasiconstant level Γ_{0j} and ΔG_{0j} in the remaining portion of the jth pulse. The gradual release of the piled-up dislocations toward the sources during the elastic relaxation process between the pulses and after the second pulse causes the gradual increase of Γ_d and ΔG_d.

A portion of the excited dislocations can be captured by obstacles in their motion back to the source. At new equilibrium positions, they will oscillate under the influence of $\sigma(x,t)$. Their contributions to Γ_d and ΔG_d are again described by equations (3) [13, 20]. However, now the total length Λ_{ir} (or number N_{ir}) of the irreversibly displaced dislocation segments with length L_{ir} is a function of the stress amplitude σ_j at the end of jth rf pulse: $\Lambda_{ir}(\sigma_j) = N_{ir}(\sigma_j)L_{ir}(\sigma_j)$. Correspondingly, the phase memory $\Omega\tau$ is also contained in $\Lambda_{ir}(\sigma_2)$ at the end of the second pulse.

Let us assume that all the segments have the same length L. N_{ir} depends on σ_j, which is considered as a constant during the pulse, and on the pulse width t_j. Furthermore, we assume that this time dependence of N_{ir} satisfies a first-order kinetic equation

$$\dot{N}_{ir} = T_r^{-1}[N_\infty(\sigma_j) - N_{ir}] \tag{4}$$

with relaxation time T_r. Parameter $N_\infty(\sigma_j)$ is given by

$$N_\infty(\sigma_j) = N_0 \int_0^{\sigma_j} n(\sigma_{loc})\,\mathrm{d}\sigma_{loc} \tag{5}$$

where N_0 is the total number of segments and $n(\sigma_{loc})$ is the distribution of local stresses σ_{loc} overcome by moving dislocations. We take $n(\sigma_{loc})$ of a quadratic form

$$n(\sigma_{loc}) = \frac{3}{4\sigma_d^3}(-\sigma_{loc}^2 + 2\sigma_i\sigma_{loc} + \sigma_d^2 - \sigma_i^2) \tag{6}$$

with two parameters σ_d and σ_i. Under the above assumptions, equation (4) is easily solved. Since Λ_{ir} is constant in time after the second pulse, $\Delta G_{ir} \sim \Lambda_{ir}$ and $\Delta\Gamma_{ir} \sim \Lambda_{ir}$ obtained from equations (3) by substitution of Λ_{ir} for Λ provide the existence of the memory echoes.

Finally, dislocations in piezoelectrics are charged and surrounded by a charged cloud. When the dislocation moves with respect to the cloud, an electric dipole is formed. An irreversible displacement of dislocation line leads to quasistatic polarization and it can give contributions both to the two-pulse echoes and the three-pulse memory echoes through electrostriction [13, 14]. This 'field–mode interaction' is operative during the applied pulses. It is not taken into account here, since the piling up of the dislocations suppresses this mechanism. Note, however, that in the case of integration under the successive pulse pairs, electrostriction can be one of the important mechanisms for memory echoes.

Thus, we approximate G and Γ in equation (1) by amplitude-independent G_{j0} and Γ_{j0}, respectively, during the pulses. Furthermore, on the basis of qualitative arguments given

above, we approximate G and Γ during the free relaxation by expressions

$$G = G_0 - \Delta G_{ir}(s_j) - a_{\omega 1} s(x,t) + a_{\omega 2} s^2(x,t) \tag{7}$$

$$\Gamma = \Gamma_0 + \Delta\Gamma_{ir}(\sigma_j) + \alpha_{\Gamma 1}\sigma(x,t) - \alpha_{\Gamma 2}\sigma^2(x,t) \tag{8}$$

respectively. At the end of the jth pulse where $\sigma(x,t) = \sigma_j$, equations (7) and (8) give $G = G_{j0}$ and $\Gamma = \Gamma_{j0}$, respectively. For $t = \infty$, these expressions describe the irreversible contributions only, since $\sigma(x,\infty) = 0$.

3. General expression for the two-pulse rf echoes

On substitution of expressions (7) and (8) into equation (1) it describes the elastic strains $s = s_e(x,t)$ in the particle. As usual [2], we approximate all particles of the sample by a platelet of thickness $2d$, with surface normal oriented at an angle ϕ relative to the externally applied field $E(t) = \mathrm{i}E_j \exp(-\mathrm{i}\omega_0 t + \mathrm{i}\phi_j)$, and assume that the effective field, $E_j \cos\phi$, couples to the thickness-shear vibrations of the platelet via the linear piezoelectric constant e and the nonlinear electrostriction constant γ_6 (2). In the slowly varying envelope approximation, the solution to equation (1) is taken in the form

$$s(x,t) = a(t)m(x)\exp(-\mathrm{i}\omega_0 t) \tag{9}$$

where $a(t)$ is a dimensionless slowly varying amplitude and $m(x)$ is a normal mode function. For our choice of the normal mode $m(x) = (\pi/2)\cos(\pi x/2d)$. In obtaining $N_{ir}(\sigma_j)$ from (4)–(6), it is sufficient to restrict oneself to the linear solution to equation (1). That is, we put $\sigma_1 = G_0 a_1 m(x)$ for the first pulse and $\sigma_{12} = G_0 a_{12} m(x)$ for the second pulse, where

$$\begin{aligned}
&a_j = \beta E_j t_j \qquad \beta = \beta_0 \cos\phi \qquad \beta_0 = -\frac{e(\varepsilon_0/\varepsilon)\cos\phi}{2\rho\omega_0 d^2(1+K^2)} \\
&a_{12}^2 = a_1^2\,\mathrm{e}^{-2\Gamma_0\tau} + a_2^2 + 2a_1a_2\,\mathrm{e}^{-\Gamma_0\tau}\cos(\omega\tau - \varphi) \\
&\omega = \omega_0 - \Omega_0 \qquad \Omega_0^2 = \frac{\pi^2}{4}\frac{G}{\rho}\frac{1+K^2}{d^2}.
\end{aligned} \tag{10}$$

Here, K is the electromechanical coupling constant, ε_0 is the free space permittivity, and ε is the dielectric constant of the piezoelectric material. As usual [9], we put $\varphi_1 = 0$ and $\varphi_2 = \varphi$.

Making use of expressions (2), (4)–(6) and (9) in equation (1) and after the proper integration over x, the resulting nonlinear equation for $a(t)$ in the slowly varying envelope approximation is

$$\dot{a} + (\Gamma_{sj} - \mathrm{i}\omega_{sj})a + (A_1 - \mathrm{i}B_1)|a|a - (A_2 - \mathrm{i}B_2)|a|^2 a = \beta E_j\,\mathrm{e}^{\mathrm{i}\varphi} + \mathrm{i}\eta E_j^2\,\mathrm{e}^{\mathrm{i}2\varphi}a^* \tag{11}$$

$$\Gamma_{s1} = \Gamma_0 + \Gamma_{dL}(1-f_1)c(a_1) \qquad \omega_{s1} = \omega + \Delta\Omega_{dL}(1-f_1)c(a_1)$$

$$\Gamma_{s2} = \Gamma_0 + \Gamma_{dL}[(1-f_1)f_2 c(a_1) + (1-f_2)c(a_{12})]$$

$$\omega_{s2} = \omega + \Delta\Omega_{dL}[(1-f_1)f_2 c(a_1) + (1-f_2)c(a_{12})]$$

$$c(x) = c_0 + c_1 x + c_2 x^2 + c_3 x^3 \qquad \eta = \eta_0\cos^2\phi \qquad \eta_0 = \frac{\gamma_6\Omega_0}{2G}\left(\frac{\varepsilon_0/\varepsilon}{1+K^2}\right)^2$$

$$f_j = \mathrm{e}^{-t_j/T_r} \qquad A_1 = (4/3)\alpha_{\Gamma 1}G_0 \qquad B_1 = (\pi^2/6d^2)\alpha_{\omega 1}G_0/\rho\Omega_0$$

$$A_2 = \frac{3\pi^2}{16}\alpha_{\Gamma 2}G_0^2 \qquad B_2 = \frac{3\pi^4\alpha_{\omega 2}G_0^2}{128d^2\rho\Omega_0}.$$

Here Γ_{dL} and $\Delta\Omega_{dL} = (\Omega/2G)\Delta G_{dL}$ are given by equations (3) with l replaced by L. In the case of distribution (6) one has

$$c_0 = \frac{1}{2}\left(1 + \frac{\sigma_i^3}{2\sigma_d^3} - \frac{3\sigma_i}{2\sigma_d}\right) \qquad c_1 = \frac{3G}{4\sigma_d^3}(\sigma_d^2 - \sigma_i^2)$$
$$c_2 = \frac{3G^2\sigma_i}{4\sigma_d^3} \qquad c_3 = -\frac{G^3}{4\sigma_d^3}. \tag{12}$$

We seek the solution of equation (11) with the right-hand side set equal to zero as

$$a(t) = a(t_j)\exp[-(\Gamma_{sj} - \mathrm{i}\omega_{sj})t - \psi_j^{re}(t) + \mathrm{i}\psi_j^{im}(t)] \tag{13}$$

where $a(t_j)$ is the amplitude at the end of the jth pulse. An approximate solution asymptotically exact both for $t \to 0$ and $t \to \infty$ and qualitatively correct everywhere over the interval is

$$\psi_j^{re}(t) = \ln|(h_j + \mathrm{e}^{\Gamma_{sj}t} - 1)/h_j| - \Gamma_{sj}t$$
$$\psi_j^{im}(t) = \omega_{sj}t + \frac{\psi_j^{re}(t)h_j|a(t_j)|}{\Gamma_{sj}(1-h_j)}\left[B_1 + \frac{B_2h_j|a(t_j)|}{(1-h_j)}\right] - \frac{B_2|a(t_j)|^2(1-\mathrm{e}^{-\Gamma_{sj}t})}{\Gamma_{sj}(1-h_j)}\,\mathrm{e}^{-\psi_j^{re}(t)} \tag{14}$$
$$h_j = \Gamma_{sj}/\Gamma_j \qquad \Gamma_j = \Gamma_{sj} + A_1|a(t_j)| - A_2|a(t_j)|^2.$$

As noted above, during the pulses we use the following equation:

$$\dot{a} + (\Gamma_{0j} - \mathrm{i}\omega_j)a = \beta E_j\,\mathrm{e}^{\mathrm{i}\varphi} + \mathrm{i}\eta E_j^2\,\mathrm{e}^{\mathrm{i}2\varphi}a^*$$
$$\omega_j = \omega + \omega_{j0} \qquad j = 1, 2 \tag{15}$$

where ω_{j0} is related to G_{j0}. Equation (15) is easily solved. As a result, the amplitude for $t > \tau + t_2$ is given by

$$a(t, \omega, \phi, \varphi) = a(t_2)\exp[-(\Gamma_{s2} - \mathrm{i}\omega_{s2})t'' - \Psi_2^{re}(t'') + \mathrm{i}\Psi_2^{im}(t'')] \tag{16}$$
$$a(t_2) = a_{2r} + \mathrm{i}a_{2\mathrm{i}}$$
$$a_{2r} = \frac{\mathrm{e}^{-\Gamma_{20}t_2}}{\sqrt{\eta^2E_2^4 - \omega_2^2}}\{\sqrt{\eta^2E_2^4 - \omega_2^2}\,a_{1rt'}\cosh\theta_2 - \omega_2 a_{1it'}\sinh\theta_2$$
$$+\eta E_2^2[a_{1it'}\cos 2\varphi - a_{1rt'}\sin 2\varphi]\sinh\theta_2\} + a'_{2r}\cos\varphi - a'_{2i}\sin\varphi$$
$$a_{2i} = \frac{\mathrm{e}^{-\Gamma_{20}t_2}}{\sqrt{\eta^2E_2^4 - \omega_2^2}}\{\sqrt{\eta^2E_2^4 - \omega_2^2}\,a_{1it'}\cosh\theta_2 + \omega_2 a_{1rt'}\sinh\theta_2$$
$$+\eta E_2^2[a_{1rt'}\cos 2\varphi + a_{1it'}\sin 2\varphi]\sinh\theta_2\} + a'_{2i}\cos\varphi + a'_{2r}\sin\varphi$$
$$a_{1rt'} = [a'_{1r}\cos(\omega_{s1}t' + \psi_1^{im}(t')) - a'_{1i}\sin(\omega_{s1}t' + \psi_1^{im}(t'))]\,\mathrm{e}^{-\Gamma_{s1}t' - \psi_1^{re}(t')}$$
$$a_{1it'} = [a'_{1i}\cos(\omega_{s1}t' + \psi_1^{im}(t')) + a'_{1r}\sin(\omega_{s1}t' + \Psi_1^{im}(t'))]\,\mathrm{e}^{-\Gamma_{s1}t' - \psi_1^{re}(t')}$$
$$a'_{jr} = \frac{\beta E_j}{\eta^2E_j^4 - \omega_j^2 - \Gamma_{j0}^2}[\mathrm{e}^{-\Gamma_{j0}t_j}(\sqrt{\eta^2E_j^4 - \omega_j^2}\sinh\theta_j + \Gamma_{j0}\cosh\theta_j) - \Gamma_{j0}]$$
$$a'_{ji} = \frac{\beta E_j(\eta E_j^2 + \omega_j)}{\eta^2E_j^4 - \omega_j^2 - \Gamma_{j0}^2}\left[\frac{\mathrm{e}^{-\Gamma_{j0}t_j}}{\sqrt{\eta^2E_j^4 - \omega_j^2}}(\sqrt{\eta^2E_j^4 - \omega_j^2}\cosh\theta_j + \Gamma_{j0}\sinh\theta_j) - 1\right]$$
$$a(t_1) = a'_{1r} + \mathrm{i}a'_{1i} \qquad \theta_j = \sqrt{\eta^2E_j^4 - \omega_j^2}\,t_j \qquad t' = \tau - t_1 + t_2 \qquad t'' = t - \tau - t_2.$$

Here, for $\eta^2E_j^4 < \omega_j^2$, $(\eta^2E_j^4 - \omega_j^2)^{1/2}$ is replaced by $(\omega_j^2 - \eta^2E_j^4)^{1/2}$ and the hyperbolic functions should be replaced by appropriate trigonometric ones.

The amplitude, $V_0(t, \tau, E_1, E_2, t_1, t_2, \varphi)$, and the phase, $\Psi(t, \tau, E_1, E_2, t_1, t_2, \varphi)$, of the piezoelectric response of the sample consisting of particles vibrating according to equations (16) are given by [2]

$$V(t) = V_{in}(t, \tau)\sin\omega_0 t + V_{out}(t, \tau)\cos\omega_0 t = V_0\sin(\omega_0 t + \Psi)$$
$$\sim \mathrm{Re}\left\{ -\mathrm{i}\,\mathrm{e}^{-\mathrm{i}\omega_0 t}\int_{-\infty}^{\infty}\int_0^{\pi} a(t, \tau, \omega, \phi, \varphi)G(\omega)G_R(\omega)\,\mathrm{d}\phi\sin\phi\cos\phi\,\mathrm{d}\omega\right\} \tag{17}$$

where $G(\omega)$ describes the distribution of normal mode frequencies, $G_R(\omega)$ represents the rf frequency response of the circuit and receiver.

4. Nonlinear mechanisms and general expression for two-pulse microwave echoes

Polarization echoes in piezoelectric powders at mw frequencies exhibit the dynamic properties only [2] in contrast to echoes in the rf range which consist of both the dynamic and the quasistatic memory components. As we have seen, the formation and basic properties of the rf echoes in piezoelectric powders depend to a great extent on the presence of a statistically large number of mobile dislocations produced in the particles during the grinding of the bulk material. On the other hand, experiments [2] at microwave frequencies were carried out in commercial powder samples not containing mobile dislocations. Hence, nonlinear mechanisms of other than dislocation origin are operative in this case. One of these mechanisms, nonlinear excitation, is given by the same parametric field–mode interaction (2) [2].

The other two types of nonlinearity, the amplitude dependence of the frequency, Ω, and of the damping, Γ, in dislocationless material are caused by pure lattice anharmonicity [2]. Here, we assume that the effective elastic modulus c_{eff} depends on the strain amplitude, $|s|$, in the form

$$c_{eff} = c_2 + \tfrac{1}{3}c_3|s| + \tfrac{1}{12}c_4|s|^2 + \cdots \tag{18}$$

where c_2, c_3 and c_4 are, in general, complex constants: $c_n = c_n^{re} + \mathrm{i}c_n^{im}$. Then, all these nonlinearities are described by the following expansion of the internal energy density $U(s, E)$ of a particle over the strain field, $s(x, t)$, and the internal field E_{in}:

$$U(s, E) = \tfrac{1}{2}c_{eff}s^2 - eE_{in}s + \tfrac{1}{2}\gamma_6 E_{in}^2 s^2. \tag{19}$$

Applying expansion (19) to the wave equation (1) and performing integration over x, we again obtain nonlinear equation (11) for $a(t)$ where $\omega_{sj} \equiv \omega = \omega_0 - \Omega_0$,

$$\Omega_0^2 = -\frac{c_2^{re}(1+K^2)}{\rho}\frac{\int mm_{xx}\,\mathrm{d}V}{\int m^2\,\mathrm{d}V} \qquad \Gamma_{sj} \equiv \Gamma_0 = -\frac{c_2^{im}}{2\omega_0\rho}\frac{\int mm_{xx}\,\mathrm{d}V}{\int m^2\,\mathrm{d}V}$$
$$A_1 = \frac{c_3^{im}}{2\rho\omega_0}\frac{\int\left(mm_x^2 + m^2m_{xx}\right)\mathrm{d}V}{\int m^2\,\mathrm{d}V} = -\frac{\pi^2 c_3^{im}}{12\rho\omega_0 d^2} \qquad B_1 = \frac{c_3^{re}}{c_3^{im}}A_1 \tag{20}$$
$$A_2 = -\frac{c_4^{im}}{4\rho\omega_0}\frac{\int(2m^2m_x^2 + m^3m_{xx})\,\mathrm{d}V}{\int m^2\,\mathrm{d}V} = \frac{\pi^4 c_4^{im}}{256\rho\omega_0 d^2} \qquad B_2 = \frac{c_4^{re}}{c_4^{im}}A_2.$$

Therefore, amplitude $a(t)$ for $t > \tau + t_2$ is given by the same equation (16) with $\Gamma_{0j} = \Gamma_0$ and $\omega_j = \omega$ there.

5. Numerical calculations and discussion

5.1. Radiofrequency echoes

From equation (10) one sees that $a_{12}(\omega\tau)$ as well as the contained expressions for Γ_{s2}, ω_{s2} (11) and $\psi_2^{re(im)}$ (14) are periodic in $\omega\tau$. Therefore, we may perform the Fourier expansion of $a(t, \tau, \omega, \varphi, \phi)$ with the Bessel functions as the Fourier coefficients [2, 6, 9, 13]. The insertion of this expansion into $V(t)$ (17) gives, after the integration over ω, the echoes at times $t \approx m\tau$ ($m = 2, 3, 4, \ldots$). However, the general expression obtained in this way is a very complex double integral over ω and ϕ. As a result, the analytic evaluation of the echo properties presents difficulties, especially in the important case of the large-signal limit.

On the other hand, expressions (17) are calculated easily numerically with β_0, η_0, T_r, σ_i, σ_d, Γ_0, Γ_{dL}, $\Delta\Omega_{dL}$, A_1, A_2, B_1, B_2 and the parameter of the mode distribution, T_2^* (see below) as the fitting parameters. In so doing, we consider V_0 and Ψ as functions of either pulse amplitudes E_1, E_2, pulse widths t_1, t_2, initial phase $\varphi_{12} = \varphi$, pulse separation τ or the time interval t_e between the second pulse and the echoes. The time dependence of the echo will be considered first as the most important property of any echo phenomenon.

Figure 1(a) shows the dependence of $V_0(2\tau)$ on 2τ for different values of E_1 and E_2. For comparison with the results of [2] in quartz powders, pulse widths t_1, t_2 are both taken as 6 μs. It is seen that at low amplitudes of the pulses (curve 1) the echo amplitude initially slightly decreases reaching a minimum and then increases to a maximum before decaying for large τ. At high amplitudes with $E_1 > E_2$ (curves 4, 5), the minimum is less deep and occurs at larger τ, as E_2 increases. For large values of $E_1 \leqslant E_2$ (curves 2, 3), only the decrease of V_0 with increasing τ is observed.

Figure 1(b) shows the decay behaviour for a constant ratio of E_1 to E_2 with E_1 greater than E_2 by 3 dB for different amplitudes of E_1 and E_2. The position of the minimum moves to smaller values of τ as the amplitudes decrease.

In obtaining these results, the following values of the parameters were used: $\beta_0 = 3\times10^{-5}$ m s V^{-1}, $\eta = -9\times10^{-8}$ m^2 V^{-2} s^{-1}, $T_r = 2\times10^{-3}$ s, $\sigma_i = \sigma_d = 7\times10^5$ N m^{-2}, $\Gamma_0 = 300$ s^{-1}, $\Gamma_{dL} = 1\times10^6$ s^{-1}, $\Delta\Omega_{dL} = 2\times10^6$ s^{-1}, $A_1 = 2\times10^6$ s^{-1}, $A_2 = 2\times10^{10}$ s^{-1}, $B_1 = 2.5\times10^7$ s^{-1}, $B_2 = 1.4\times10^{11}$ s^{-1}. In addition, the normal distribution of the modes

$$G(\omega) = (T_2^*/\sqrt{2\pi})\exp[-(\omega T_2^*)^2/2] \tag{21}$$

with $T_2^* = 1\times10^{-5}$ s and

$$G_R(\omega) = G_R(0)/[1 + (\omega/\omega_B)^2] \tag{22}$$

with $\omega_B = 8\pi\times10^6$ s^{-1} [2] were assumed.

The results shown in figures 1(a) and 1(b) are in good agreement with the experimental observations in quartz powders [2] and on the basis of the theory given above can be explained as follows. The contribution to the echo from the nonlinear excitation mechanism on taking damping into account has a maximum value at $\tau = 0$, but it is small for low amplitudes of the pulses. It decreases monotonically to zero with increasing τ. The contributions from the amplitude-dependent damping and dispersion are zero at $\tau = 0$ and initially increase with τ, reach a maximum and further decrease for large τ. Thus, the echo increases not from zero at $\tau = 0$ but from the value given by the nonlinear excitation mechanism.

Hence it follows that the observed minimum is a result of vectorial adding up of the contributions to the echo from all three nonlinear mechanisms with each contribution having its own time-dependent amplitude and phase. The displacement of the minimum to smaller values of τ with decreasing E_2 is caused by the amplitude dependence of G (7) and of

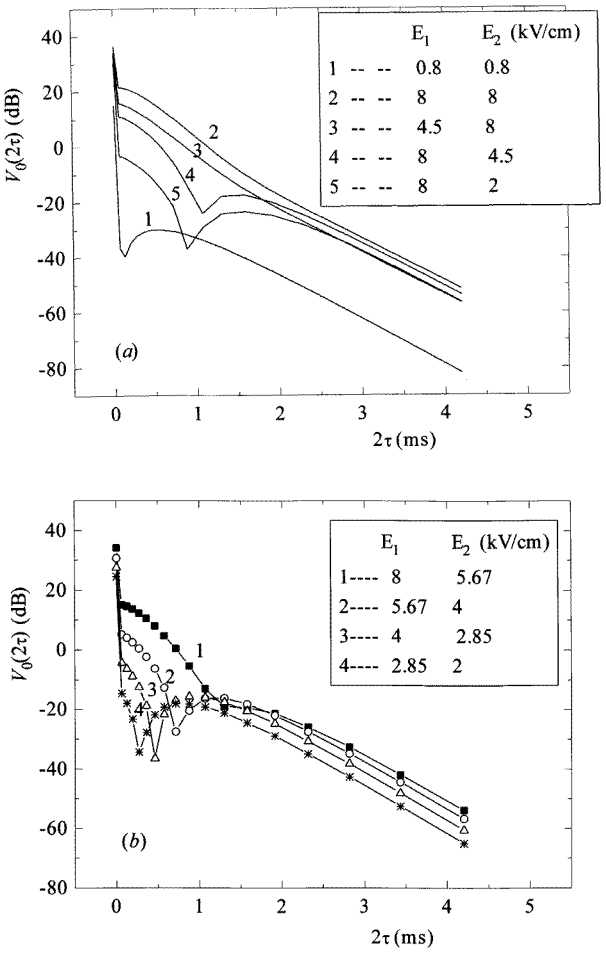

Figure 1. Decay of two-pulse rf echo, $V_0(2\tau)$, versus 2τ.

Γ (8). Indeed, normal mode frequency Ω initially decreases with increasing σ_j reaching a minimum and then increases due to the piling up of dislocations. In figure 2 the dependence of difference frequency $\omega_2 = \omega_{s2} + \mathrm{d}\Psi_2^{im}/\mathrm{d}t$ at the end of the second pulse on E_2 is shown for different values of E_1 and for several values of $\omega\tau$. As is seen from curve 1 ($E_1 = 8$ kV cm^{-1}, $\omega\tau = 0$), for large values of E_2 frequency ω_2 and its associated contribution to the echo increase with decreasing E_2. The same is true for Γ_2 and for its contribution to the echo. At the same time, the contribution to the echo from the nonlinear interaction decreases with decreasing E_2. Thus, the combined effect of all the mechanisms moves the minimum to smaller values of τ as E_2 decreases.

Plot 1 in figure 3 shows again curve 5 from figure 1(a) in arbitrary units (not in dB). Curves 2 and 3 depict the same decay picture calculated for the case of phase sensitive detection. Initial phase $\varphi_{12} = \varphi = 0$ for curve 2 and $\varphi = 0.0915$ rad for curve 3. In the last case the echo phase, Ψ, on the maximum is zero: $\Psi(\tau_{max}) = 0$. It is seen that under this condition phase reversal occurs at $\tau = \tau_{min}$ where $V_0(2\tau)$ has the minimum. (Because $\varphi \ll 1$ there is little difference between curves 2 and 3). Similar phase reversal of the echo was observed and investigated at microwave frequencies [2] (see also figure 12 below).

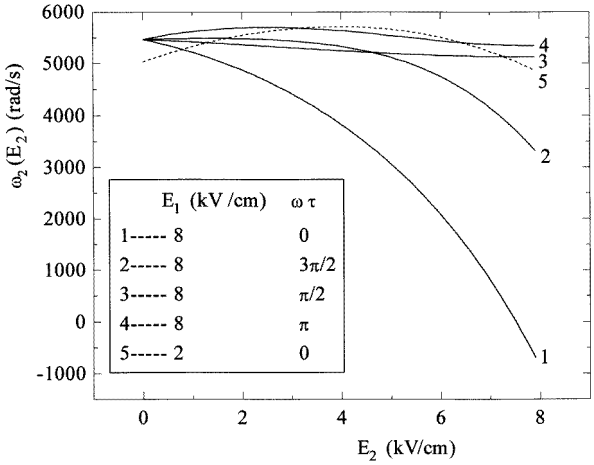

Figure 2. Difference frequency, ω_2, at the end of the second pulse, versus amplitude, E_2, of the second pulse.

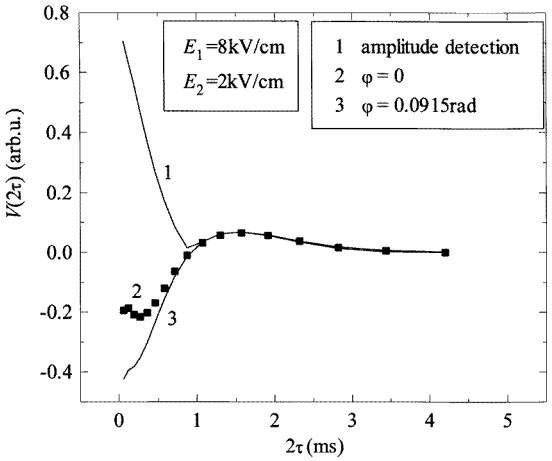

Figure 3. Amplitude and phase sensitive detection of the two-pulse rf echo.

All the following results, unless otherwise noted, are obtained with the use of the parameters given above.

In figure 4(*a*) and (*b*) we show the echo shapes and positions for several values of t_1 and t_2. Note that the echo shape essentially depends on the distribution of normal modes ω.

The dependence of $V_0(2\tau)$ on the first-pulse amplitude, E_1, is shown in figure 5 for several values of E_2. The equal pulse widths are $t_1 = t_2 = 1$ μs. In all cases $V_0(2\tau)$ is proportional to E_1 for $E_1 < E_2$ (the straight line has slope 1). For $E_1 \geqslant E_2$, $V_0(2\tau)$ reaches a maximum and then decreases with increasing E_1.

In figure 6 the dependence of $V_0(2\tau)$ on the second-pulse amplitude, E_2, for several values of E_1 is shown. Here, $V_0(2\tau)$ is proportional to E_2^2 for $E_2 < E_1$ (the straight line has slope 2), exhibits a broad maximum for $E_2 \geqslant E_1$ and decreases with further increasing

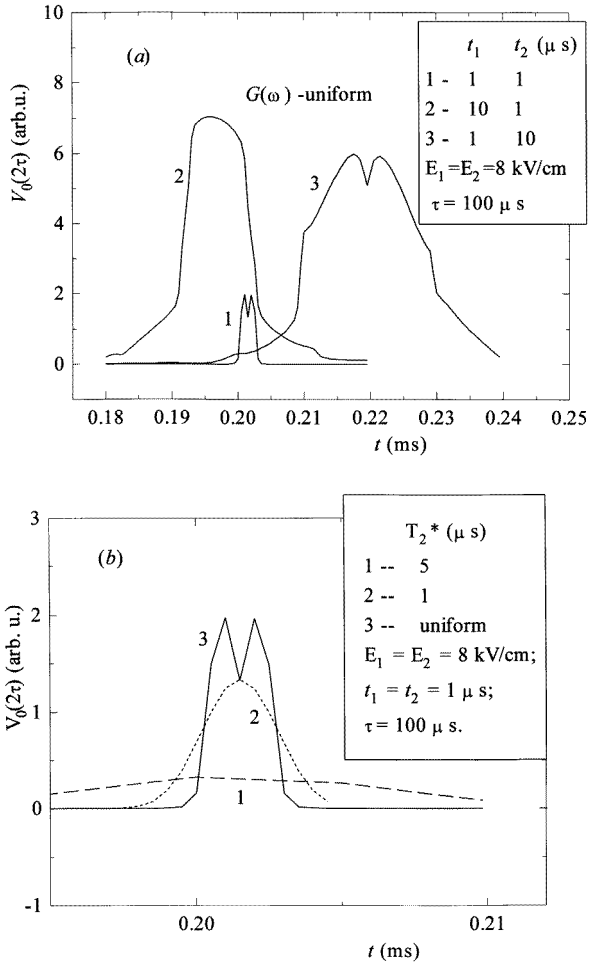

Figure 4. Two-pulse rf echo shapes and positions.

E_2. In general, the results of figures 5 and 6 are in good qualitative and fair quantitative agreement with [2, 9] everywhere over the broad range of amplitudes E_1, E_2 used in the experiments.

In order to better understand the role of the nonlinear mechanisms in echo formation, the distribution of the powder particles at various moments of time may be displayed in the plane $\{a_{in}(t), a_{out}(t)\}$ as a phase diagram [6, 20]. Such phase diagrams at $t = 2\tau$ are given in figure 7(a) and (b). Figure 7(a) shows the distributions when the echo is caused *separately* by the nonlinear excitation (curve 1), the amplitude-dependent frequency shift (curve 2) and by the amplitude-dependent damping (curve 3). Figure 7(b) depicts the phase diagrams for the linear system (curve 1) and for the echo due to all three nonlinear mechanisms operating *together* (curve 3). The diagram due to the nonlinear excitation (curve 2) is given again here for comparison. The points A_k, B_k, C_k and D_k ($k = 1, 2, 3$) on the curves are related to phase values $\omega\tau = 0 \pm n2\pi$, $\pi/2 \pm n2\pi$, $\pi \pm n2\pi$ and $3\pi/2 \pm n2\pi$, respectively ($n = 1, 2, 3, \ldots$). Note that figure 3 of [20] related to the case of nonlinear excitation is in error.

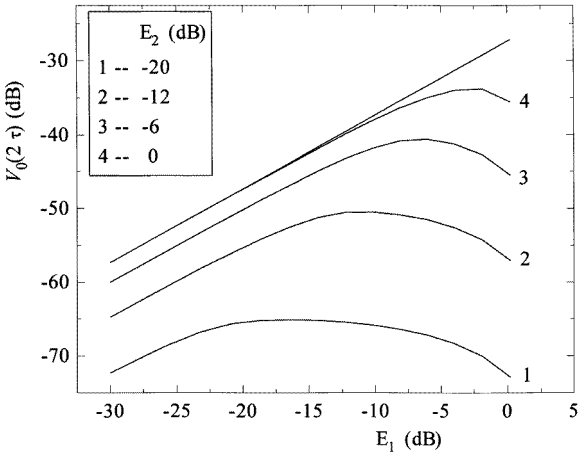

Figure 5. Two-pulse rf echo amplitude, $V_0(2\tau)$, versus first-pulse amplitude E_1.

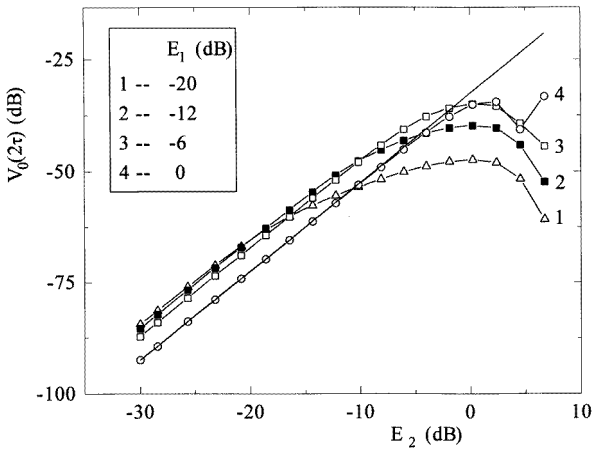

Figure 6. Two-pulse rf echo amplitude, $V_0(2\tau)$, versus second-pulse amplitude E_2.

The decay behaviour of the secondary two-pulse echo, $V_0(3\tau)$, occurring at $t = 3\tau$ and also described by expressions (16), (17) is shown in figure 8 for several values of E_1 and E_2. Here, the abscissa is the interval between the second pulse and the 3τ echo. Unlike the primary 2τ echo, the 3τ echo amplitude is first built up and then decays monotonically for different values of E_1 and E_2.

5.2. Microwave echoes

Note that there are fewer experimental observations on echoes in the microwave region in contrast to those in rf echoes. Moreover, there is some uncertainty in the magnitudes of the pulse fields used in experiments. Hence, it is not so easy to estimate the related parameters from the comparison of numerical calculations with the experimental data [2]. Therefore, the data given below present a very rough approximation to reality. In our calculations 0 dB corresponds to 35 000 V m^{-1} which in turn represents 1 kW peak power in the waveguide.

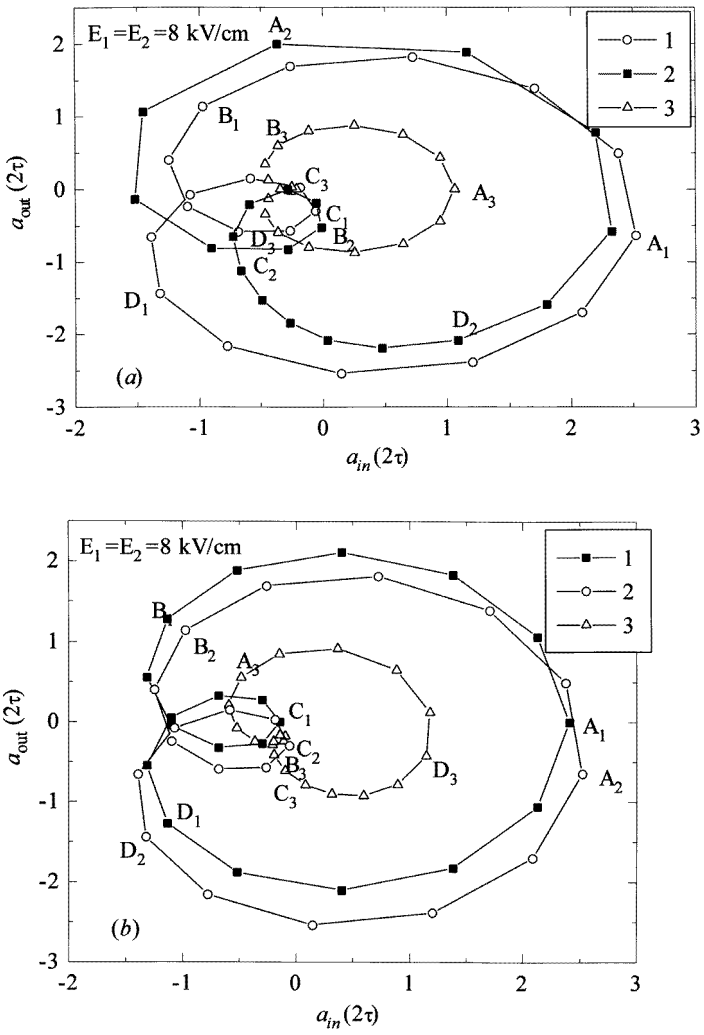

Figure 7. Distribution of powder particles (dipoles) in the phase plane at time $t = 2\tau$. Nonlinear mechanisms accounted for: (*a*) 1, nonlinear excitation, 2, amplitude-dependent dispersion and 3, amplitude-dependent damping; (*b*) 1, linear approximation, 2, nonlinear excitation and 3, all three nonlinear mechanisms.

Figure 9 shows a two-pulse echo sequence calculated for pulses of equal width and for the case of uniform mode distribution ($G(\omega) = \text{constant}$). For short pulses we have a single-peaked signal both with amplitude detection and with phase sensitive detection. The echoes are spaced equally and the primary echo occurs at time $t_e \approx 2\tau + 2t_2 - t_1$ as it must do [2, 9]. The first two echoes coincide in phase: $\Psi(2\tau) = \Psi(3\tau)$, and differ by π relative to the phases of 4τ and 5τ echoes. In general, the echo amplitudes, shapes, positions and the phases strongly depend on parameters E_1, E_2, t_1, t_2, τ and φ.

The primary-echo ($t = 2\tau$) shapes and positions are shown in more detail in figure 10(*a*)–(*c*) for $t_1 > t_2$, $t_1 < t_2$ and $t_1 = t_2$, respectively. Here, plots 1, 2 are obtained with the uniform distribution of the normal modes and plots 3, 4 are due to the normal

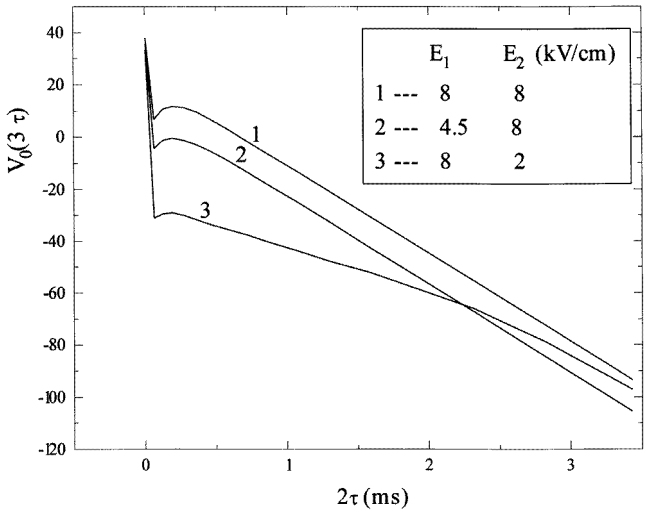

Figure 8. Decay of the secondary two-pulse rf echo, $V_0(3\tau)$, versus 2τ.

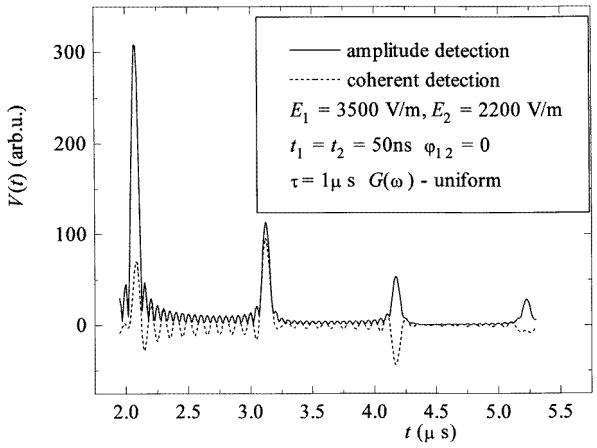

Figure 9. Two-pulse mw echo sequence.

distribution with $T_2^* = 100$ ns. Furthermore, curves 1, 3 are related to amplitude detection and curves 2, 4 to phase sensitive detection. A comparison of figure 10(*a*) with figure 44 of [2] shows that the multiple-peaked structure due to the uniform distribution more closely correlates with experiment than the single-peaked one obtained with the normal distribution. On the other hand, the picture given by the normal distribution with $T_2^* = 10$ ns (not shown in the figure) is already very much like that given by curves 1, 2.

In figure 10(*b*) we have a multiple-peaked structure with a pronounced central peak in the case of amplitude detection (plot 1) and a single-peaked one with phase sensitive detection (plot 2) if the mode distribution is uniform. The normal distribution with $T_2^* = 100$ ns gives a single-peaked picture (curves 3 and 4 in figure 10(*b*)). A single peak is observed for $t_1 < t_2$ experimentally [2].

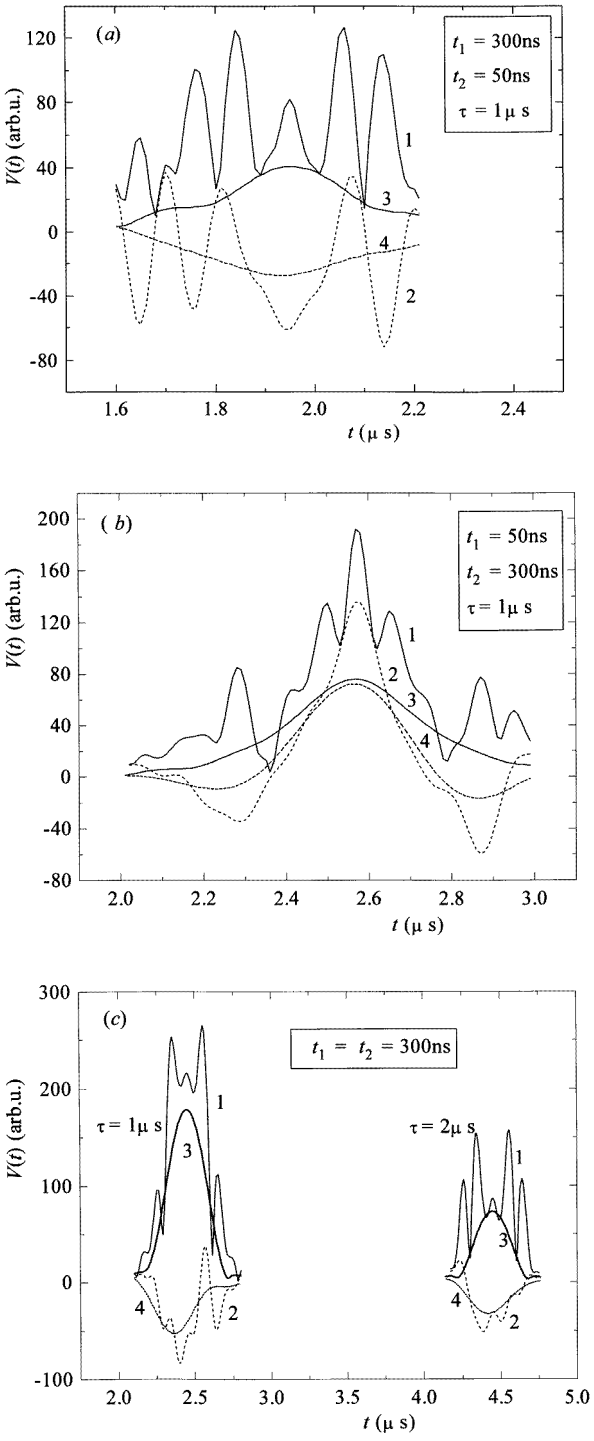

Figure 10. Primary two-pulse mw echo shapes and positions. $E_1 = 3500$ V m^{-1}, $E_2 = 2200$ V m^{-1}, $\varphi = 0$. 1, 2—uniform mode distribution, 3, 4—normal distribution with $T_2^* = 100$ ns. 1, 3—amplitude detection, 2, 4—phase sensitive detection.

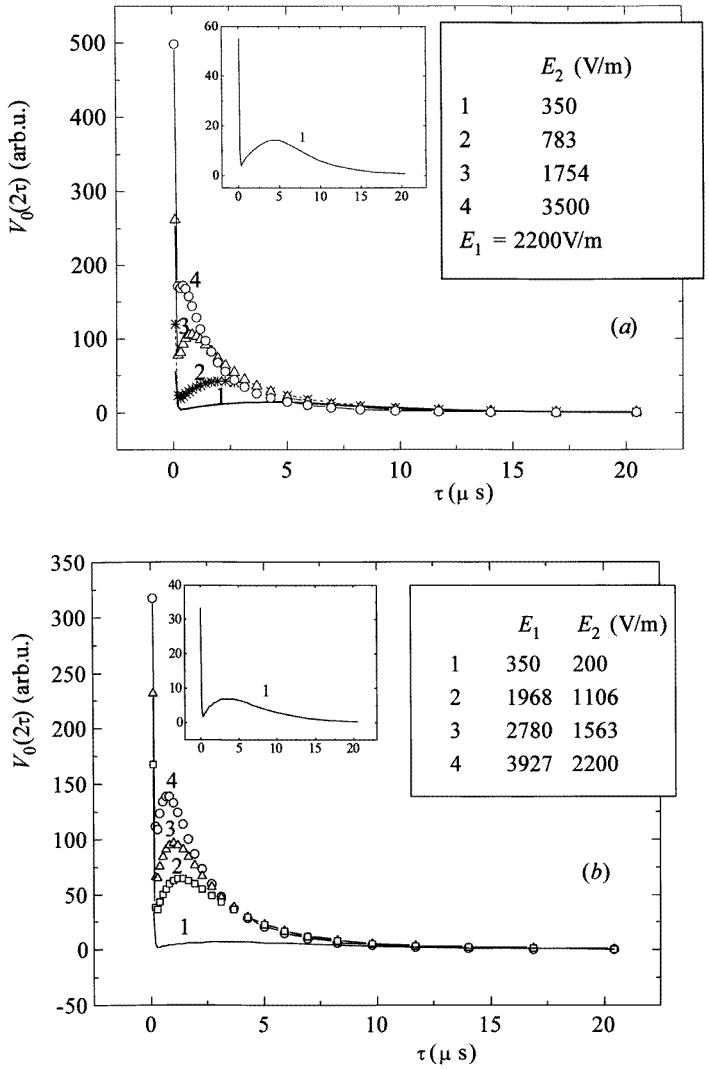

Figure 11. Decay of two-pulse mw echo, $V_0(2\tau)$, versus pulse separation τ. $t_1 = t_2 = T_2^* =$ 100 ns. Curve 1 is shown in the inset on a larger scale.

The calculated echo shapes and positions for wide pulses of equal width are shown in figure 10(*c*) for two values of τ. Note the significant changes in the echo shape when the mode distribution is uniform (curves 1 and 2).

Comparing these results with experimental observations [2], one can conclude that for wide second pulses the echo shape is mainly controlled by modes with small values of $|\omega|$.

The results shown in figures 9 and 10 as well as other results below are obtained by use of the following parameters: $\beta_0 = 0.1$ ms V^{-1}, $\eta_0 = 1\times10^{-4}$ m^2 V^{-2} s^{-1}, $\Gamma_0 = 1\times10^5$ s^{-1}, $A_1 = 2\times10^{10}$ s^{-1}, $A_2 = 1.2\times10^{12}$ s^{-1}, $B_1 = 5\times10^{10}$ s^{-1} and $B_2 = 2\times10^{12}$ s^{-1}. Putting in formulae (20) $\omega_0 = 2\pi\times9\times10^9$ rad s^{-1}, $\rho = 5600$ kg m^{-3} (ZnO) and $d = 1\times10^{-7}$ m, one has $c_3^{re} \approx -2\times10^{11}$, $c_3^{im} \approx -8\times10^{10}$, $c_4^{re} \approx 2\times10^{13}$ and $c_4^{im} \approx 1\times10^{13}$ (all in N m^{-2}).

The decay behaviour is shown in figure 11(a) for several values of E_2. It is seen that for $E_2 < E_1$ (curves 1–3) there is a sharp minimum in the decay curve followed by a maximum before monotonic decaying for large τ. The position of the maximum is a function of E_2: the maximum occurs at smaller τ as E_2 increases. For $E_2 > E_1$ (curve 4) only the decrease in amplitude V_0 for increasing τ is obtained.

The decay curves in figure 11(b) are obtained for several values of E_1 and E_2 with E_1 greater than E_2 by 5 dB. In contrast to the experimental observations (see figure 39 in [2]), here the maximum moves to smaller τ when the fields are increased.

The calculated echo decay behaviour of figure 11(a) agrees with the experimental observations in ZnO powders [2]. It can be interpreted similarly to the rf echoes above as a combined effect of the three nonlinear mechanisms. The contribution to the echo from the nonlinear excitation mechanism on taking damping into account has a maximum value at $\tau = 0$, but is small ($\sim E_1 E_2^2$) for low pulse fields (note that the small echo at $\tau \approx 0$ is masked by strong linear ringing signal). The contributions from the amplitude-dependent dispersion ($\sim B_k$) and damping ($\sim A_k$) are zero at $\tau = 0$ and initially increase with τ, reach a maximum and further decrease for large τ. The minimum observed in [2] corresponds to the resultant of the three contributions each of which has its own time-dependent amplitude and phase. At large values of E_2 the time dependence of the echo for small τ is controlled by the contribution of the nonlinear excitation and the minimum disappears.

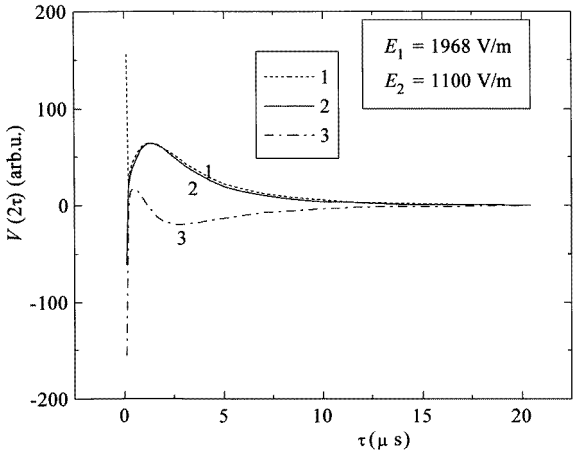

Figure 12. Amplitude (1) and phase sensitive (2, 3) detection of the mw echo. 2, $\varphi = 0.421$ rad, 3, $\varphi = 0$.

Figure 12 deals again with curve 2 from figure 11(b). Here, curve 1 is obtained with amplitude detection, and curves 2 and 3 are results of phase sensitive detection. (The initial value, $V(\tau = 0)$, is reduced for convenience.) Initial phase $\varphi = 0$ for curve 3 and $\varphi = 0.421$ radians for curve 2 when the echo phase, Ψ, on the maximum is zero: $\Psi(\tau_{max}) = 0$. It is seen that the echo envelope with phase sensitive detection strongly depends on φ. In particular, phase reversal at τ_{min} takes place if phase sensitive detection is adjusted for zero phase on the maximum, in agreement with experiment [2]. Note that because of the nonlinear character of the echo, $V_0(2\tau_{max})$ and τ_{max} also somewhat depend on φ.

The dependence of $V_0(2\tau)$ on first-pulse amplitude E_1 is shown in figure 13 for several values of E_2. The straight line with slope 1 is also given for comparison. It is seen that at the

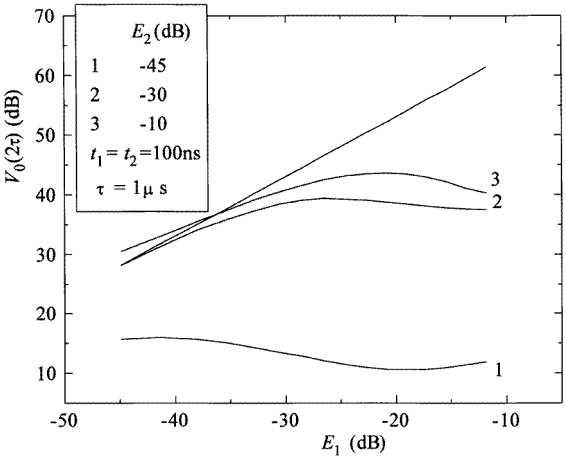

Figure 13. Two-pulse mw echo amplitude, $V_0(2\tau)$, versus first-pulse amplitude E_1.

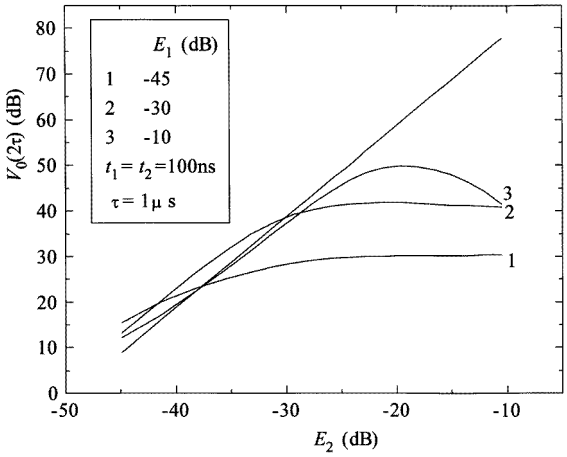

Figure 14. Two-pulse mw echo amplitude, $V_0(2\tau)$, versus second-pulse amplitude E_2.

lowest values of E_2 the echo initially depends only weakly on small values of E_1, slightly decreases with E_1 in the intermediate region and slowly increases at large E_1 (curve 1). For larger E_2, the echo increases with E_1, exhibits a maximum and further decreases. With increasing E_2, the maximum is shifted to larger values of E_1 (curves 2 and 3).

In figure 14 the dependence of $V_0(2\tau)$ on E_2 is shown for different values of E_1. At the lowest values of E_1 the echo is roughly proportional to E_2^2 in the initial region (the straight line has slope 2) and is saturated at the highest levels of E_2. For large values of E_1, $V_0(2\tau)$ exhibits a maximum before decreasing with increasing E_2. We do not know any experimental data on the amplitude dependence of the two-pulse echoes in microwave region.

6. Conclusions

In this paper we elaborate a specific qualitative dislocation model and a phenomenological theory for the amplitude-dependent dispersion and damping as nonlinear mechanisms for the rf polarization echoes in powders. For the mw echoes, we take into consideration as an origin of the nonlinearities both the important terms ($\sim c_3 s^3$ and $\sim c_4 s^4$) in the expansion of the internal energy density of a particle over the strain, s, *jointly*. Then, considering *together* all three known types of nonlinear mechanism, theories of both the rf and the mw polarization echoes in piezoelectric powders were developed. The numerical analysis of the general expressions for the echoes was employed successfully to explain the experimentally observed time, amplitude and phase properties of the two-pulse echoes, in particular, in quartz powders (rf echoes) and in ZnO powder (mw echoes). As a result, several important material parameters relevant to the nonlinear mechanisms are estimated.

Quartz is distinguished from other piezoelectrics by its better acoustic characteristics. In particular, it is seen from the fitting parameters given above that in SiO_2 the frequency change far exceeds the dislocation damping. One might expect that this factor is responsible for the minimum in the decay curve. In other materials these two values may be of the same order or the damping may even exceed the frequency change. This circumstance may be the cause for the lack of the minimum, say, in decay curves for the echoes in GaAs and $LiNbO_3$ powders [2]. Indeed, our calculations show that the decay curves obtained for equal values of the two quantities (that is, for $A_k = B_k$ in equation (11)) do not contain any minimum after the initial increase.

Supposedly [13], in ferroelectrics and in ferromagnetics all three types of nonlinearity are due, mainly, to the motion of domain boundaries. Perhaps, the disappearance of the echo in ferromagnetic powders at $H_0 > H_c$ [21] confirms this point of view.

Of course, a decrease of the particle sizes leads to the decrease of the number of dislocations (domains) in it. At the same time, important changes in the pinning forces and in the mobility of these defects are expected herewith. Hence, it will be very informative to study the dynamic and the quasistatic properties of the polarization echoes in powder samples prepared by the successive sifting through a set of sieves of the same powder material obtained during the grinding of the crystal.

In conclusion we emphasize that most of the important properties of polarization echoes in piezoelectric powders are described for the first time at least in good qualitative agreement with experimental observations over the broad range of amplitudes and widths of the excitation pulses and pulse separations by the use of one and the same set of numerical values of parameters appearing in the theory. It is hoped that the given theory coupled with more detailed experimental work will be in a position to explain the properties of the echoes also quantitatively.

Acknowledgments

The authors thank N Ya Asadullina for her significant contribution to this paper. The work was supported by grants No RKA 000 and No RKA 300 from the International Science Foundation.

References

[1] Kessel' A R, Safin I A and Gol'dman A M 1970 *Fiz. Tverd. Tela* **12** 3070 (Engl. transl. 1971 *Sov. Phys.–Solid State* **12** 2488)

[2] Fossheim K, Kajimura K, Kazyaka T G, Melcher R L and Shiren N S 1978 *Phys. Rev.* B **17** 964
[3] Herrmann G F, Hill R M and Kaplan D E 1967 *Phys. Rev.* **156** 118
[4] Bun'kov Yu M and Dmitriev V V 1981 *Zh. Eksp. Teor. Fiz.* **80** 2363
[5] Kroll S, Xu E Y, Kim M K, Mitsunaga M and Kachru R 1990 *Phys. Rev.* B **41** 11 568
[6] Gould R W 1969 *Am. J. Phys.* **37** 585
[7] Fedders P A and Lu E Y C 1973 *Appl. Phys. Lett.* **23** 502
[8] Popov S N, Krainik N N and Smolensky G A 1975 *Pis. Zh. Eksp. Teor. Fiz.* **21** 543 (Engl. transl. 1975 *Sov. Phys.–JETP Lett.* **21** 253)
[9] Berezov V M, Bashkov V I, Korepanov V D and Romanov V S 1977 *Zh. Eksp. Teor. Fiz.* **69** 1674 (Engl. transl. 1977 *Sov. Phys.–JETP* **42** 851)
[10] Kessel' A R 1978 *Ferroelectrics* **22** 759
[11] Asadullin Ya Ya 1980 *Pis. Zh. Eksp. Teor. Fiz.* **32** 405 (Engl. transl. 1980 *Sov. Phys.–JETP Lett.* **32** 380)
[12] Asadullin Ya Ya 1987 *Ukrain. Fiz. Zh.* **32** 1391
[13] Asadullin Ya Ya 1992 *Polarization Echo and Its Application* (Moscow: Nauka) p 110 (in Russian)
[14] Melcher R L and Shiren N S 1982 *Physical Acoustics* vol 16, ed W P Mason and R N Thurston (New York: Academic) p 341
[15] Kosevich A M and Bogoboyashchii V V 1982 *Fiz. Tverd. Tela* **24** 3110
[16] Pacult Z A, Riedi P C and Tunstall D P 1973 *J. Phys. F: Met. Phys.* **3** 1843
[17] Kupca S and Searle C W 1975 *Can. J. Phys.* **53** 2622
[18] Granato A V and Lucke K 1956 *J. Appl. Phys.* **27** 583
[19] Hikata A, Han M and Elbaum C 1985 *J. Phys. Coll.* **46** C5 11
[20] Asadullin Ya Ya and Samartsev V V 1993 *Izv. VUZ. Fiz.* **36** 20 (Engl. transl. 1994 *Russian Phys. J.* **36** 623)
[21] Melcher R L and Shiren N S 1976 *Phys. Lett.* **57A** 377